Structural discrimination via density functional theory and lattice dynamics: Monoclinic Mg_2NiH_4

J. F. Herbst and L. G. Hector, Jr.
Materials and Processes Laboratory, General Motors R&D Center, Mail Code 480-106-224, 30500 Mound Road Warren, Michigan 48090-9055, USA

(Received 4 February 2009; revised manuscript received 12 March 2009; published 16 April 2009)

Two distinct crystal structures for the monoclinic, low-temperature phase of Mg_2NiH_4, which we designate as LTI and LTII, are available in the published literature. We demonstrate that density functional theory and lattice dynamics can easily identify LTII as the preferable structure at two levels of inquiry. First, enthalpies of formation ΔH calculated using three different forms for the exchange-correlation energy functional are in better agreement with experiment for LTII. Second, the phonon spectrum calculated for LTII contains no anomalies while that for LTI exhibits a variety of soft modes. By analyzing the soft modes in LTI as well as those we find for the known $CaMgNiH_4$ structure with Ca replaced by Mg we derive a crystal structure that closely approximates LTII.

DOI: 10.1103/PhysRevB.79.155113 PACS number(s): 71.20.−b

I. INTRODUCTION

Since the original demonstration by Reilly and Wiswall[1] that it forms via the reversible reaction of the binary intermetallic Mg_2Ni with H_2, Mg_2NiH_4 has remained of interest as a hydrogen storage medium. Its 3.6 mass % gravimetric hydrogen density is markedly greater than that of $LaNi_5H_6$ (1.4 mass %) but substantially below the 7.6 mass % value for MgH_2. In favorable comparison to the latter material, however, it features a lower hydrogen desorption temperature (~523 K vs ~573 K for MgH_2) and faster kinetics. Many experimental studies have aimed to improve these properties, which are still insufficient for demanding applications such as mobile storage, via elemental substitutions, additions, and preparation by various methods (see, e.g., Refs. 2–5 and references therein).

Mg_2NiH_4 is a semiconductor and forms an ordered low-temperature (LT) monoclinic phase and a disordered high-temperature cubic modification. In this paper we focus on the LT form, for which two structural determinations from neutron-diffraction studies of the deuterated analog are available: (a) the $C2/m$ (space group No. 12) structure of Noréus and Werner,[6] which we designate as LTI, and (b) the $C2/c$ (space group No. 15) structure of Zolliker *et al.*,[7] to which we refer as LTII. Aside from their common monoclinic lattice symmetry, the two structures are qualitatively distinct. The unit cell of LTI contains 4 Mg_2NiD_4 formula units (f.u.) with planar NiD_4 nearest-neighbor groups having an Ni atom centered in a rectangular quartet of D atoms,[6] while LTII contains 8 f.u. per unit cell with D atoms surrounding the Ni atoms in a tetrahedral configuration.[7] Figure 1 illustrates the structures.

We demonstrate that density functional theory (DFT) can establish conclusively that LTII is preferable at both the electronic and vibrational levels of analysis. First, the densities of electronic states indicate that LTII is semiconducting while LTI is metallic and the LTII total electronic energies afford better comparison to the measured enthalpy of hydride formation, ΔH. In order to assess the impact of the exchange-correlation energy functional ε_{xc} in DFT on the calculated ΔH and its accuracy vis-à-vis experiment, we derive electronic energies using three different approximations for ε_{xc}. Second, the phonon spectra calculated for LTII exhibit no anomalies, whereas those for LTI are characterized by soft modes signaling lattice instability.

II. COMPUTATIONAL METHODS

Electronic energies for this study were obtained with the Vienna *ab initio* simulation package (VASP), which implements DFT (Ref. 8) with a plane-wave basis set.[9,10] Potentials constructed by the projector-augmented wave (PAW) approach[11,12] were employed for the elements. The three approximations utilized for ε_{xc} were (i) the local-density approximation (LDA) of Ceperley and Alder[13] as parameter-

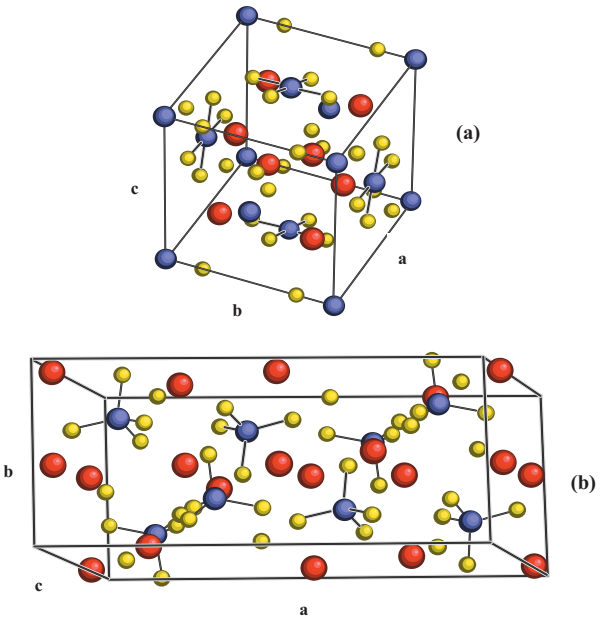

FIG. 1. (Color) Unit cells of monoclinic (a) LTI ($C2/m$) and (b) LTII ($C2/c$) Mg_2NiH_4 crystal structures (Mg–red; Ni–blue; H–yellow).

ized by Perdew and Zunger,[14] (ii) the generalized gradient approximation (GGA) of Perdew and Wang (PW91),[15,16] and (iii) the GGA of Perdew, Burke, and Ernzerhof (PBE);[17] the latter two in conjunction with the interpolation formula of Vosko *et al.*[18] A plane-wave cutoff energy of at least 900 eV was imposed. Lattice constants and nuclear coordinates were relaxed, together, at least twice. The energy of the H_2 molecule was calculated in a $12\times13\times14$ Å^3 box, large enough to ensure isolation. In all cases the electronic total energy was converged to 10^{-6} eV/cell and the force components on each atom relaxed to less than 10^{-3} eV/Å. Reciprocal space k-point meshes having spacings in the 0.09–0.13 Å^{-1}, 0.10–0.18 Å^{-1}, and 0.05–0.14 Å^{-1} ranges were used for LTI, LTII, and Mg_2Ni (hexagonal $P6_222$ structure[19]), respectively. Phonon spectra for the solids and the vibrational frequency of the H_2 molecule were computed with the direct method for lattice dynamics,[20] employing VASP as the computational engine.

III. ELECTRONIC RESULTS: DENSITY OF STATES AND ΔH_{el}

All three approximations for ε_{xc} indicate that Mg_2Ni and Mg_2NiH_4 (LTI) are metallic while Mg_2NiH_4 (LTII) is semiconducting. Figure 2 displays the densities of states (DOSs) obtained with PW91; for Fig. 2 as well as Fig. 6 below the linear tetrahedron method was employed, retaining the k meshes used in the relaxations. The LTI DOS disagrees with experiment since Mg_2NiH_4 is known to be a semiconductor, so that even at this stage it can be concluded that the LTII structure is more appropriate for the hydride. Another pronounced distinction is that the valence-band gap in LTII [Fig. 2(b)] vanishes in LTI [Fig. 2(a)]. The LTII DOS is very similar to those calculated and discussed in detail by van Setten *et al.*,[21] also using PW91, and by Häussermann *et al.*,[22] employing ultrasoft pseudopotentials. In particular, the gap between the valence and conduction bands in Fig. 2(b) is 1.56 eV. This is in excellent agreement with the 1.6 eV (1.54 eV) result obtained in Ref. 21 (Ref. 22). In the LDA (PBE) we find the gap to be 1.48 (1.54) eV. The DFT values somewhat underestimate the 1.68–2.0 eV measurements[23–25] of the gap, as is usually the case.

From the electronic total energies E_{el} we can derive ΔH_{el}, the enthalpy of hydride formation at zero temperature in the absence of zero-point energy (ZPE) contributions

$$\Delta H_{el}(Mg_2NiH_4) = E_{el}(Mg_2NiH_4) - E_{el}(Mg_2Ni) - 2E_{el}(H_2). \quad (1)$$

The values given in Table I demonstrate that ΔH_{el} for LTII, in the PW91 approximation for ε_{xc}, is in best accord with measurements of the formation enthalpy ΔH_{298} (expt.). Our $\Delta H_{el}=-63.8$ kJ/mole H_2 result for LTII (PW91) agrees with the $-64(-63)$ kJ/mole H_2 values from other theoretical predictions in Ref. 21 (Ref. 22). For each ε_{xc} in Table I ΔH_{el} for LTII is much more negative than that for LTI, implying that the tetrahedral NiH_4 configuration in LTII is more stable than the planar arrangement in LTI. The semiconducting behavior of LTII [Fig. 2(b)] is intimately linked to the presence of the tetrahedral 18-electron $(NiH_4)^{4-}$-type complexes (cf. the discussion in Ref. 22). In LTI the more stable tetrahedral form is not developed and the metallic nature of the Mg_2Ni parent compound is retained [Figs. 2(a) and 2(c)]. It is clear that the electronic levels unambiguously point to LTII as the preferable structure.

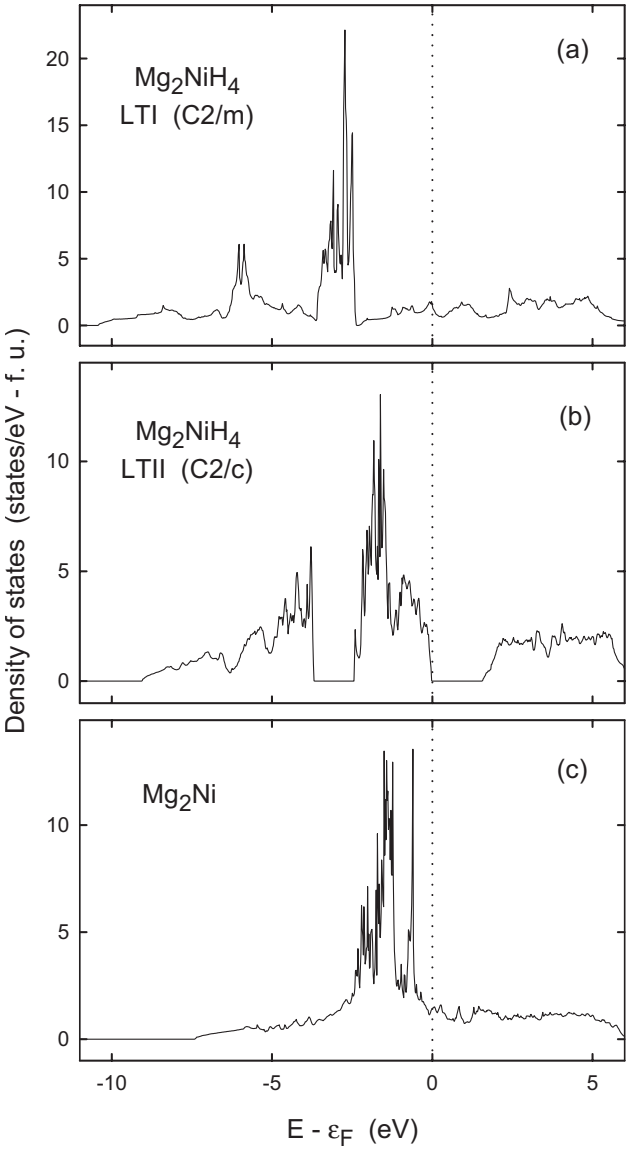

FIG. 2. Electronic DOS calculated in the GGA (PW91) for (a) Mg_2NiH_4 (LTI), (b) Mg_2NiH_4 (LTII), and (c) Mg_2Ni. (a) LTI and (c) Mg_2Ni feature finite DOS at the Fermi level ε_F and are thus metallic, while LTII is semiconducting.

IV. PHONONS

Our calculated phonon spectra also identify LTII as more favorable than LTI. In all three ε_{xc} approximations LTI produces soft modes with substantial imaginary frequencies, signaling lattice instability, while all LTII spectra exhibit no anomalies. Phonon dispersion relations and corresponding total phonon DOS obtained with PW91 are displayed in Fig. 3 (LTI) and Fig. 4 (LTII). The first step of each phonon

TABLE I. Enthalpies of formation ΔH and their components calculated as defined by Eqs. (1)–(3) for Mg_2NiH_4 and experimental values ΔH_{298} (expt.). All values in kJ/mole H_2.

	LDA	GGA-PW91	GGA-PBE
	LTI ($C2/m$)		
ΔH_{el}	−79.6	−27.9	−22.9
	LTII ($C2/c$)		
ΔH_{el}	−110.4	−63.8	−57.3
ΔH_{ZPE}	11.3	9.5	9.5
ΔH_0	−99.1	−54.3	−47.7
$\delta\Delta H_{298}$	−7.3	−7.1	−7.1
ΔH_{298}	−106.3	−61.3	−54.8
ΔH_{298} (expt.)		−64.5 [a] −68 [b]	

[a]Reference 1.
[b]Reference 26.

calculation involved geometry optimization of a supercell of suitable size constructed from the fully optimized conventional cell. Based upon this optimized supercell, N perturbed supercells of the same size were constructed, where N is the number of crystallographically independent displacements of the constituent atoms necessary for determining the spectrum of phonon frequencies $\omega_{\vec{q}}$. Separate VASP single-point energy calculations were conducted on each perturbed supercell. For LTI the phonon calculation involved $N=42$ $2\times2\times2$ supercells, each containing 224 atoms. For LTII $N=48$ $1\times2\times2$ supercells, each containing 224 atoms, were required. Atomic displacements of ±0.02 Å for each perturbed supercell were found to be satisfactory. Tests with larger supercells and smaller and larger atomic displacements revealed no significant differences in the reported vibrational energies.

A. ΔH_{298} for LTII

Vibrational contributions to the enthalpy of hydride formation ΔH can be derived for LTII since the phonon spectrum (Fig. 4) confirms lattice stability. At temperature T we write

$$\Delta H_T = \Delta H_{el} + \Delta H_{ZPE} + \delta\Delta H_T, \tag{2}$$

where ΔH_{el} is the electronic component given by Eq. (1). ΔH_{ZPE} is the zero-point energy contribution specified by the analog of Eq. (1) with E_{el} replaced by E_{ZPE} $(=\frac{1}{2}\Sigma_{\vec{q}}\hbar\omega_{\vec{q}}$ for the solids, $\frac{1}{2}\hbar\omega_0$ for H_2, with ω the vibrational frequencies). $\delta\Delta H_T$ is the correction to finite T,

$$\delta\Delta H_T(Mg_2NiH_4) = E_{ph}(Mg_2NiH_4) - E_{ph}(Mg_2Ni) - 2\left[\frac{7}{2}kT + E_{vib}(H_2)\right], \tag{3}$$

where $E_{ph}=\Sigma_{\vec{q}}\hbar\omega_{\vec{q}}n(\omega_{\vec{q}})$ is the phonon energy without the ZPE, $n(\omega)=(e^{\hbar\omega/kT}-1)^{-1}$, $\frac{7}{2}kT$ is the sum of the translational $(\frac{3}{2}kT)$, rotational (kT), and $pV=kT$ energies for H_2, and $E_{vib}=\hbar\omega_0 n(\omega_0)$ is its vibrational energy. The $T=0$ enthalpy of formation is $\Delta H_0=\Delta H_{el}+\Delta H_{ZPE}$. Table I lists ΔH_{298} (LTII) and its components in the three approximations for ε_{xc}. ΔH_{ZPE} and $\delta\Delta H_{298}$ are small in comparison to ΔH_{el} and do not depend significantly on the ε_{xc} used in the phonon work; moreover, the two enter ΔH_{298} with opposite signs and largely cancel. PW91 leads to the best agreement with the measured values; interestingly, ΔH_{el} alone is in slightly better accord with experiment than ΔH_{298}. We note that the volume dependence of the ZPE has been ignored. Its effect on the ground-state energy and lattice parameters can be appreciable for light element systems, as we showed explicitly for LiH (Ref. 27) and for Be and BeH_2 (Ref. 28), but we fully expect its impact on Mg_2NiH_4 to be negligible. We

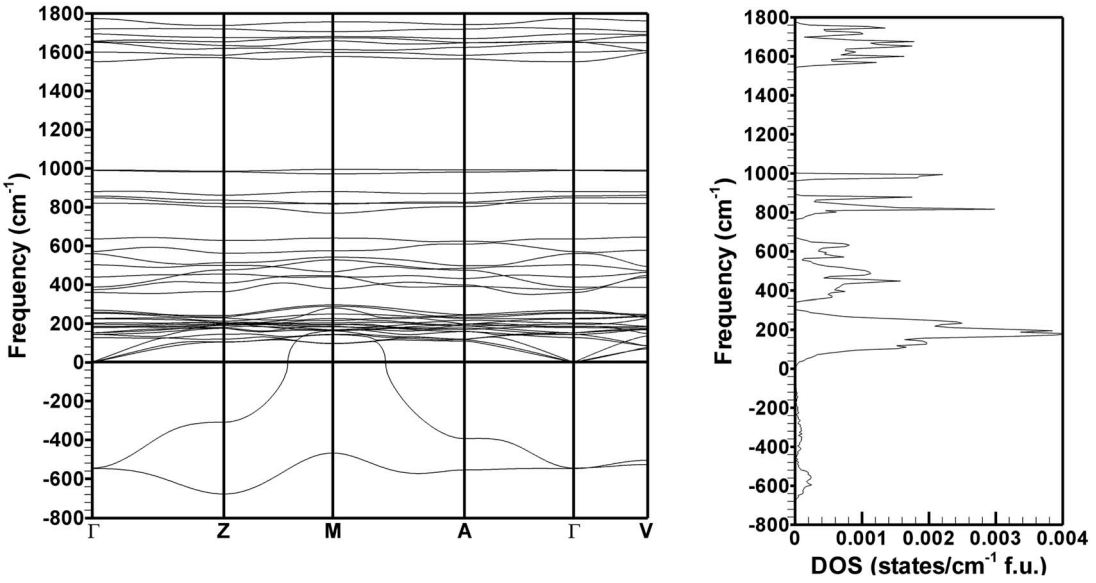

FIG. 3. Phonon spectrum (left) and corresponding phonon DOS (right) calculated in the GGA (PW91) for $C2/m$ Mg_2NiH_4 (LTI). Imaginary frequencies are plotted as negative.

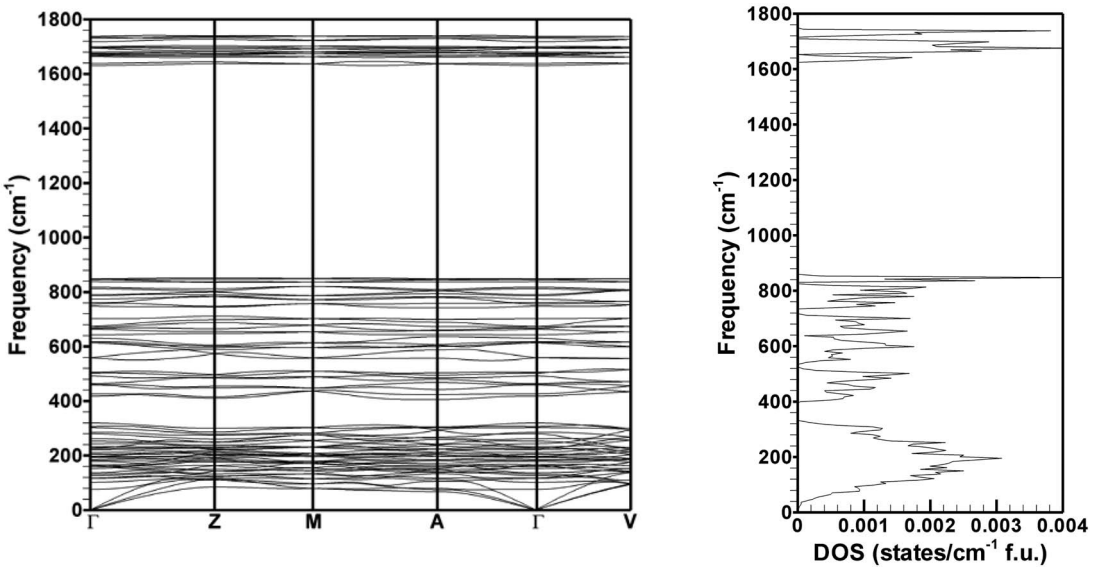

FIG. 4. Phonon spectrum (left) and corresponding phonon DOS (right) calculated in the GGA (PW91) for $C2/c$ Mg_2NiH_4 (LTII). No instabilities are noted.

estimate the precision of each calculated ΔH_{298} in Table I to be roughly ± 3 kJ/mole H_2.

B. Exploring soft modes

We investigated the possibility of deriving the LTII crystal structure via the analyses summarized below of soft modes obtained not only from LTI (Fig. 3) but also from the cubic $CaMgNi_2H_4$ structure[29] with Mg substituted for Ca. Our strategy was to first optimize each experimental structure with VASP, calculate its phonon dispersion curves, capture the soft-mode crystal structures at the high-symmetry points and optimize them, identify the structure having the lowest electronic total energy E_{el}, compute its phonon dispersion relations, and iterate in this way until a structure having a stable phonon spectrum was obtained. Supercell sizes for each structure were chosen to ensure that interactions between equivalent ions in periodic images, as well as the force constants computed at the boundaries of each supercell, were negligible. All calculations described below were made in the PW91 GGA.

1. LTI

Eight distinct monoclinic structures were captured from the nine soft modes at the high-symmetry points in Fig. 3 and optimized with VASP. The two A-point structures are identical, and there are two modes at Γ whose small separation (3 cm^{-1}) is not discernible in Fig. 3. We find the following space group, number Z of Mg_2NiH_4 f.u. per unit cell, and total electronic energy E_{el} in eV per Mg_2NiH_4 for each of these structures: (1) lower (i.e., more negative frequency as plotted in Fig. 3) soft mode at Γ: Cm (No. 8), $Z=4$, $E_{el}=-23.27$; (2) upper (i.e., more positive frequency in Fig. 3) soft mode at Γ: $C2$ (No. 5), $Z=4$, $E_{el}=-23.27$; (3) lower soft mode at Z: $C2/m$, $Z=8$, $E_{el}=-23.62$; (4) upper soft mode at Z: $C2/m$, $Z=8$, $E_{el}=-23.45$; (5) single soft mode at M: $C2/m$, $Z=8$, $E_{el}=-23.27$; (6) either soft mode at A: $C2/m$, $Z=4$, $E_{el}=-23.13$; (7) lower soft mode at V: $C2/c$, $Z=8$, $E_{el}=-23.27$; (8) upper soft mode at V: $C2/m$, $Z=8$, $E_{el}=-23.26$. All E_{el} values are below $E_{el}=-23.13$ eV/Mg_2NiH_4 calculated for LTI with the exception of those for the two A-point structures, which are equal to it. Although the structure from the lower V point is characterized by the same $C2/c$ space group as LTII, its unit cell contains 8 f.u. and it does not produce the lowest E_{el}. The lower soft mode at Z in Fig. 3 has the largest $|\omega_{\vec{q}}|$ and the $C2/m$ structure acquired from it features the lowest E_{el}, 0.26 eV above the -23.88 eV/Mg_2NiH_4 value for LTII. Significantly, it is a semiconductor, as is LTII, while the other soft-mode structures are all metallic.

The vibrational spectrum of the monoclinic $C2/m$ structure corresponding to the lower soft mode at the Z point in Fig. 3 was computed in a phonon calculation using $N=60$ $2\times2\times2$ supercells. Each supercell comprised 448 atoms. The phonon dispersion relations revealed eight soft modes at the high-symmetry points (one each at Γ and Z, two each at M, A, and V) and seven distinct structures (the two from the A point are again identical). On optimization with VASP we find that all are semiconductors and all E_{el} are equal to or below $E_{el}=-23.62$ eV/Mg_2NiH_4 obtained for the antecedent lower Z-point structure. The triclinic $P\bar{1}$ (No. 2) structure captured from the soft mode at Γ, for which $|\omega_{\vec{q}}|$ is greatest, yields the lowest E_{el} (-23.75 eV/Mg_2NiH_4), 0.13 eV above that for LTII. The cell volume is $V=66.7$ Å^3/Mg_2NiH_4, and there are two distinct Ni sites, each enclosed by a flattened irregular tetrahedron of H atoms with d(Ni-H) bond distances and H-Ni-H angles in the 1.54–1.57 Å and 102.9°–132.3° ranges for one and 1.53–1.57 Å and 98.4°–147.9° for the other. Aside from the Ni-H bond lengths, these do not compare very favorably to LTII, whose optimized $V=68.1$ Å^3/Mg_2NiH_4, 1.55 Å $< d$(Ni-H) <1.58 Å, and the H-Ni-H bond angle range is 107.6°–116.3°, with all but the largest angle within ~2.5°

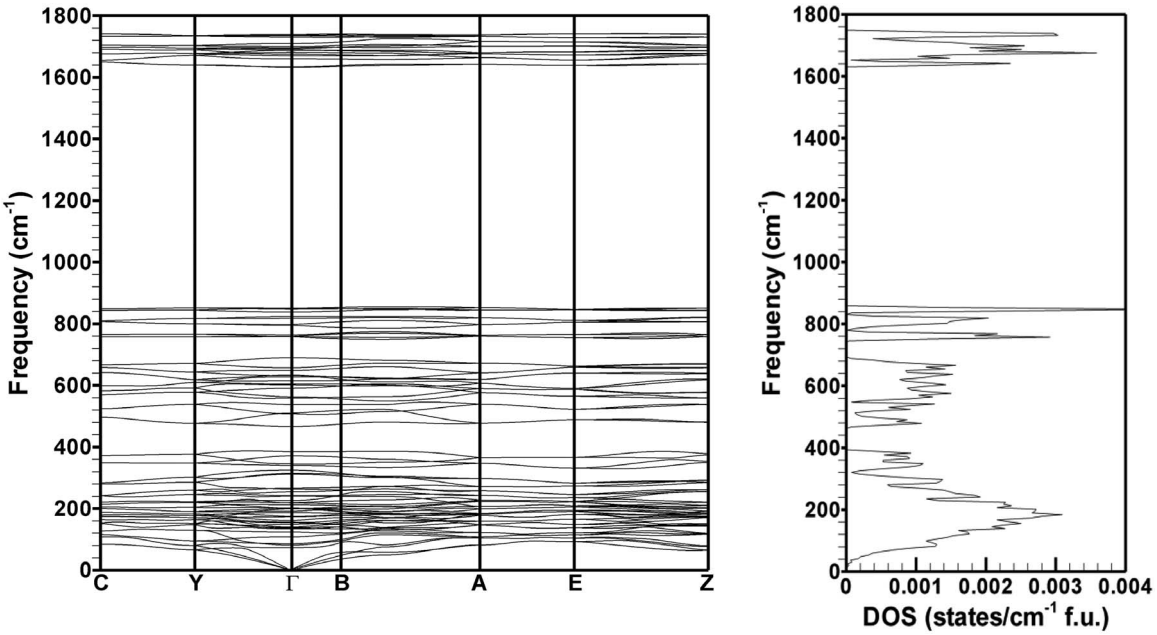

FIG. 5. Phonon spectrum (left) and corresponding phonon DOS (right) calculated in the GGA (PW91) for $P2_1$ Mg_2NiH_4. No instabilities are noted.

of the 109.5° value for a perfect tetrahedron. The phonon spectrum calculated ($N=84$ 242-atom $2\times2\times2$ supercells) of this $P\bar{1}$ structure contains no instabilities, and we conclude that it is the structure most closely approximating LTII that can be derived from analysis of the soft modes in LTI.

2. *Mg-substituted* $CaMgNiH_4$

In an additional effort to derive LTII from a related experimental structure we calculated the phonon spectrum for the cubic ($P2_13$; space group No. 198; $Z=4$) $CaMgNiH_4$ structure[29] after substituting Mg for Ca to simulate Mg_2NiH_4. For the phonon calculation $N=14$ $2\times2\times2$ perturbed supercells, each containing 224 atoms, were constructed from the VASP-optimized conventional cell. The phonon dispersion relations exhibit a rich array of soft modes; at the Γ, R, M, and X high-symmetry points there are 3, 2, 4, and 4 such modes, respectively. One mode at Γ and another at X are characterized by the same and largest value of $|\omega_{\vec{q}}|$. We captured crystal structures only from these modes, building on our experience with LTI in Sec. IV B 1 by assuming they will lead to the minimum electronic total energies E_{el}. The structure from the mode at Γ is monoclinic ($P2_1$; No. 4) with a compact unit cell ($Z=4$, 28 atoms) while that from X is triclinic ($P1$; No. 1) with a huge unit cell ($Z=32$, 224 atoms). Both were optimized with VASP, yielding $E_{el}=-23.85(-23.78)$ eV/Mg_2NiH_4 for the $P2_1$ ($P1$) structure, each below $E_{el}=-23.70$ eV/Mg_2NiH_4 for the $CaMgNiH_4$-type precursor. For the $P2_1$ structure a phonon calculation involving $N=84$ $2\times2\times2$ supercells, each consisting of 224 atoms, yielded the phonon dispersion relations and total phonon DOS in Fig. 5. These reveal no instabilities.

With E_{el} only 0.03 eV/Mg_2NiH_4 (3 kJ/mole Mg_2NiH_4) above that for LTII, the $P2_1$ structure is energetically the closest to LTII that can be derived from our soft-mode analyses of LTI and Mg-substituted $CaMgNiH_4$. Table II presents its lattice constants and atomic position parameters. The cell volume is within 1% of that for LTII, and each of the two Ni

TABLE II. Optimized lattice parameters and atomic positions for the monoclinic ($P2_1$; No. 4) Mg_2NiH_4 structure obtained from soft-mode analyses as described in text. All atoms are on 2*a* sites.

Unit-cell parameters			
a(Å)	6.514	α(°)	90.0
b(Å)	6.398	β(°)	95.8
c(Å)	6.508	γ(°)	90.0
	V(Å^3/Mg_2NiH_4)	67.47	

Atomic position parameters			
Atom	x	y	z
Mg1	0.9743	0.2516	0.2345
Mg2	0.4672	0.2660	0.8333
Mg3	0.5332	0.7281	0.6667
Mg4	0.0255	0.7430	0.2655
Ni1	0.2311	0.0249	0.0362
Ni2	0.2313	0.4696	0.5361
H1	0.3730	0.9367	0.8754
H2	0.9962	0.4812	0.4688
H3	0.2745	0.2313	0.5651
H4	0.2744	0.2633	0.0646
H5	0.0038	0.5134	0.0313
H6	0.3726	0.5572	0.3743
H7	0.7165	0.0663	0.2456
H8	0.7169	0.4287	0.7452

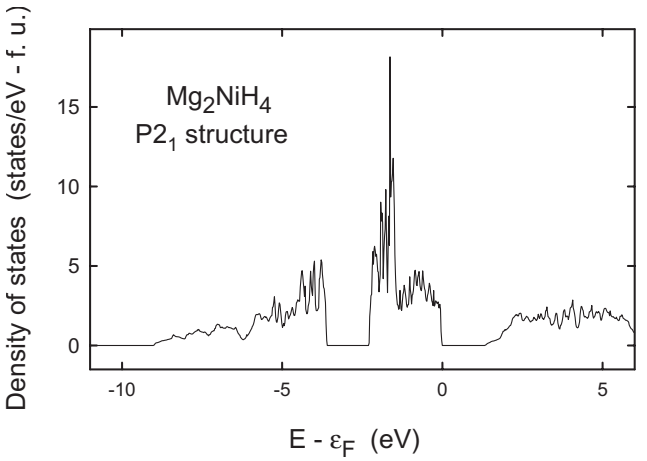

FIG. 6. Electronic density of states calculated in the GGA (PW91) for the Mg_2NiH_4 monoclinic $P2_1$ crystal structure obtained as described in text.

sites is surrounded by a tetrahedron of H atoms only slightly more distorted than that in LTII, with 1.55 Å $< d$(Ni-H) $<$ 1.57 Å and Ni-H-Ni bond angles in the 104.0°–115.1° range. The phonon spectrum and DOS in Fig. 5 and the electron DOS in Fig. 6 for the $P2_1$ structure closely resemble those of LTII [Figs. 2(b) and 4, respectively]. The $P2_1$ structure is a semiconductor with a computed band gap of 1.27 eV, somewhat smaller than the 1.56 eV gap for LTII also calculated using PW91. The computed ZPEs of the two structures are in very close proximity: 0.84 eV/Mg_2NiH_4 for $P2_1$ vs 0.85 eV/Mg_2NiH_4 for LTII. We obtain $\Delta H_{298} = -60.4$ kJ/mole H_2 for $P2_1$, a value departing only marginally from the −61.3 kJ/mole H_2 result for LTII in Table I.

For comparison purposes Fig. 7 presents neutron powder-diffraction diagrams calculated at a wavelength of 1.54 Å for LTII and for the $P2_1$ and $P\bar{1}$ structures derived from our soft-mode analyses of LTI and Mg-substituted $CaMgNiH_4$, respectively. The VASP-optimized (PW91) structural parameters were employed in each case; for LTII [Fig. 7(a)] the pattern is essentially the same as that for the experimental structure since the structural parameters differ negligibly from those observed.[7] The $P2_1$ structure clearly leads to a pattern [Fig. 7(b)] in qualitatively better agreement with that for LTII than does the $P\bar{1}$ model [Fig. 7(c)], consistent with our finding that the energy of the $P2_1$ structure approaches that of LTII more closely.

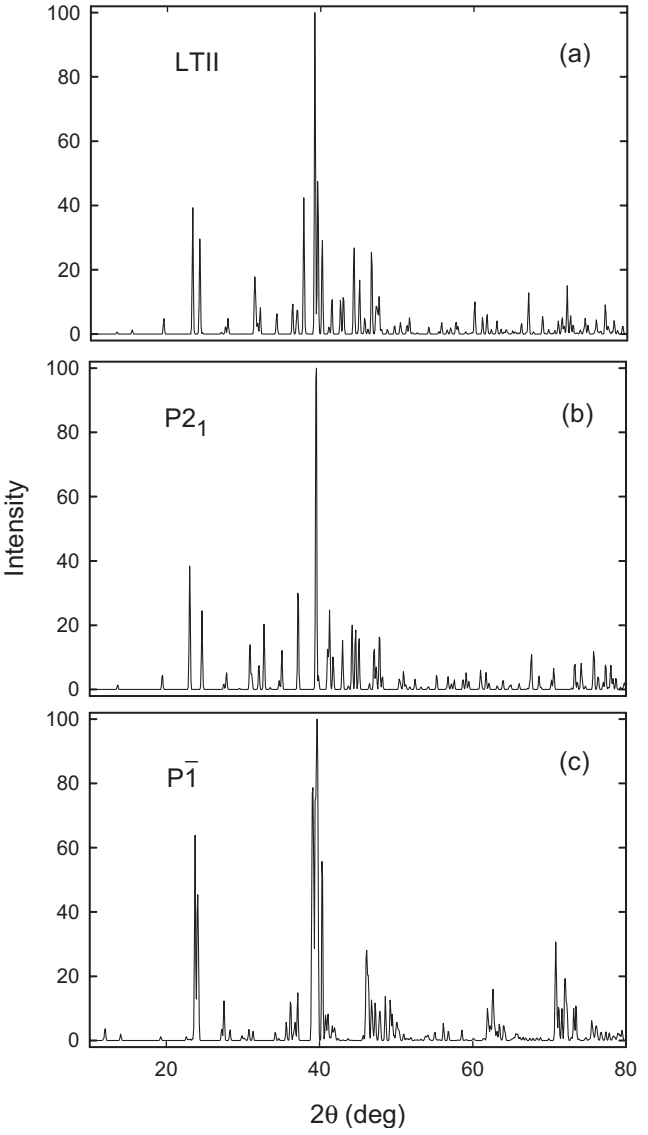

FIG. 7. Neutron diffraction diagrams calculated for (a) LTII (monoclinic $C2/c$), (b) the monoclinic $P2_1$ structure derived from analyzing soft modes in Mg-substituted $CaMgNiH_4$, and (c) the triclinic $P\bar{1}$ structure obtained from following soft modes in LTI as described in text.

V. SUMMARY REMARKS

We have shown that DFT can easily distinguish the LTI and LTII Mg_2NiH_4 structures at both the electronic and vibrational levels of analysis. The phonon spectrum calculated for LTI (Fig. 3) is clearly anomalous, and the formation enthalpy obtained for LTII in the PW91 GGA is in best agreement with experiment (Table I).

Via investigation of soft modes in LTI and Mg-substituted $CaMgNiH_4$ we identified a monoclinic structure (Table II) quite similar to LTII in several respects. Given that (i) it is slightly higher in energy than LTII and (ii) the phases in the Mg_2NiH_4 system have been well-determined experimentally, it is in our opinion an excellent approximation to LTII but not another phase that might exist between 300 K and the monoclinic-cubic transition at ~500 K. Our work demonstrates that soft-mode analyses can provide, at a minimum, approximate structures sufficient for deriving accurate energetics.

ACKNOWLEDGMENT

We are grateful to P. Saxe for stimulating and useful discussions.

[1] J. J. Reilly and R. H. Wiswall, Inorg. Chem. **7**, 2254 (1968).
[2] S. Bouaricha, J. P. Dodelet, D. Guay, J. Huot, S. Boily, and R. Schulz, J. Alloys Compd.. **307**, 226 (2000).
[3] A. Zaluska, L. Zaluski, and J. O. Ström-Olsen, Appl. Phys. A: Mater. Sci. Process. **72**, 157 (2001).
[4] E. Grigorova, M. Khristov, M. Khrussanova, and P. Peshev, J. Alloys Compd. **414**, 298 (2006).
[5] X. Liu, Y. Zhu, and L. Li, J. Alloys Compd. **425**, 235 (2006).
[6] D. Noréus and P.-E. Werner, J. Less-Common Met. **97**, 215 (1984).
[7] P. Zolliker, K. Yvon, J. D. Jorgensen, and F. J. Rotella, Inorg. Chem. **25**, 3590 (1986).
[8] W. Kohn and L. Sham, Phys. Rev. **140**, A1133 (1965).
[9] G. Kresse and J. Hafner, Phys. Rev. B **49**, 14251 (1994).
[10] G. Kresse and J. Furthmüller, Comput. Mater. Sci. **6**, 15 (1996).
[11] P. E. Blöchl, Phys. Rev. B **50**, 17953 (1994).
[12] G. Kresse and D. Joubert, Phys. Rev. B **59**, 1758 (1999).
[13] D. M. Ceperley and B. J. Alder, Phys. Rev. Lett. **45**, 566 (1980).
[14] J. P. Perdew and A. Zunger, Phys. Rev. B **23**, 5048 (1981).
[15] J. P. Perdew and Y. Wang, Phys. Rev. B **45**, 13244 (1992).
[16] J. P. Perdew, J. A. Chevary, S. H. Vosko, K. A. Jackson, M. R. Pederson, D. J. Singh, and C. Fiolhais, Phys. Rev. B **46**, 6671 (1992).
[17] J. P. Perdew, K. Burke, and M. Ernzerhof, Phys. Rev. Lett. **77**, 3865 (1996).
[18] S. H. Vosko, L. Wilk, and M. Nusair, Can. J. Phys. **58**, 1200 (1980).
[19] P. Villars, *Pearson's Handbook—Desk Edition* (American Society for Metals, Materials Park, OH, 1997), p. 2338.
[20] K. Parliński, Software PHONON, Cracow (2001), as implemented in MEDEA 2.2 Materials Design (2005).
[21] M. J. van Setten, G. A. de Wijs, and G. Brocks, Phys. Rev. B **76**, 075125 (2007).
[22] U. Häussermann, H. Blomqvist, and D. Noréus, Inorg. Chem. **41**, 3684 (2002).
[23] D. Lupu, R. Sârbu, and A. Biriş, Int. J. Hydrogen Energy **12**, 425 (1987).
[24] P. Selvam, B. Viswanathan, and V. Srinivasan, J. Electron Spectrosc. Relat. Phenom. **46**, 357 (1988).
[25] D. Lupu, R. Grecu, and S. I. Fărcaş, Z. Phys. Chem. **181**, S143 (1993).
[26] M. L. Post and J. J. Murray, J. Less-Common Met. **134**, 15 (1987).
[27] J. F. Herbst and L. G. Hector, Jr., Phys. Rev. B **72**, 125120 (2005).
[28] L. G. Hector, Jr., J. F. Herbst, W. Wolf, P. Saxe, and G. Kresse, Phys. Rev. B **76**, 014121 (2007).
[29] F. Gingl and K. Yvon, Z. Kristallogr. **207**, 247 (1993).